Quantum chemical studies of hydrate formation of H_2SO_4 and HSO_4^-

Theo Kurtén[1], Madis Noppel[2], Hanna Vehkamäki[1], Martta Salonen[1] and Markku Kulmala[1]

[1] *Department of Physical Sciences, P.O. Box 64, FI-00014 University of Helsinki, Finland*
[2] *Institute of Environmental Physics, University of Tartu, 18 Ülikooli Str., 50090 Tartu, Estonia*

We calculate structures and thermochemical parameters for $H_2SO_4 \bullet (H_2O)_n$, $HSO_4^- \bullet (H_2O)_n$, $H_2SO_4 \bullet NH_3 \bullet (H_2O)_m$ and $HSO_4^- \bullet NH_3 \bullet (H_2O)_m$ clusters (with $n = 0 \ldots 4$ and $m = 0 \ldots 1$) using the MP2/aug-cc-pV($D + d$)Z quantum chemical method, with higher-order corrections computed at the MP2/aug-cc-pV($T + d$)Z and MP4/aug-cc-pV($D + d$)Z levels. Equilibrium constants for hydrate formation at different temperatures are computed using the quantum chemical results, and the predicted extent of hydrate formation is compared with experimental results. Hydrate distributions in different RH conditions are derived using the calculated free energies of hydration. The results show that the hydrogensulfate ion is in all conditions much more strongly hydrated than the neutral sulfuric acid molecule. The high-level thermodynamic data calculated for the clusters agree with the experimental data, and the presented hydrate model is expected to perform better than earlier versions based on less reliable quantum chemical data. A comparison to the ammonia-containing clusters indicates that ammonia probably plays at most a minor role in ion-induced nucleation involving the HSO_4^- core ion.

Introduction

Over the past decade or so, aerosol formation was observed at a large number of sites around the world (Kulmala *et al.* 2004). Such observations were performed on different platforms (ground, ships, aircraft) and over different time periods (campaign or continuous-type measurements). It has been proposed, and confirmed by observations, that atmospheric new particle formation depends on the sulfuric acid concentration (for example Weber *et al.* 1996, Weber *et al.* 1997, Kulmala *et al.* 2006). In laboratory experiments (Viisanen *et al.* 1997, Bernd *et al.*

2005), this dependence was found to obey a power-law form having exponents of order 4–10. In atmospheric conditions, the dependence is not as strong (for example Weber *et al.* 1996, Weber *et al.* 1997, Kulmala *et al.* 2006), with the exponent of only 1–2.

However, it has not yet been resolved what the most important nucleation mechanisms in the atmosphere are. The most realistic candidates are (*see* for example Kulmala *et al.* 2000, O'Dowd *et al.* 2002, Kulmala 2003, Lee *et al.* 2003, Lovejoy *et al.* 2004): (1) homogeneous binary water–sulfuric acid nucleation (for example in industrial plumes and in the free troposphere), (2)

homogeneous ternary water-sulfuric acid-ammonia nucleation (for example in the continental boundary layer), (3) ion-induced nucleation of binary (water–sulfuric acid) or ternary inorganic vapours or of organic vapours (for example in the upper troposphere and lower stratosphere), and (4) barrierless (kinetically controlled) homogeneous nucleation of, for example, iodine species (in coastal environments). Mechanisms 2 and 3 can also be kinetically limited. All these mechanisms have been observed in laboratory conditions, although the concentrations used in laboratory studies are typically far above those in the atmosphere. Laboratory studies (Couling *et al.* 2003a, 2003b) have also demonstrated that the initial stages of sulfate aerosol formation is likely to involve sulfuric acid hydrate clusters with one or two water molecules per acid.

Atmospheric new particle formation might actually be a two-step process (*see* for example Kulmala *et al.* 2000). The first step would be the nucleation process itself, producing atmospheric (neutral or ion) clusters. The second step would be the activation of clusters (Kulmala *et al.* 2006). The first step could also include the recombination of atmospheric ion clusters.

In the first step, ternary homogeneous nucleation seems to be thermodynamically possible in many atmospheric conditions (Anttila *et al* 2005). Also ion-induced nucleation has been shown to contribute to observed particle formation events for example in boreal forest regions (Laakso *et al.* 2006). However, the precise identities of the participating ionic and neutral molecular species are as yet unknown. Laboratory measurements (Froyd and Lovejoy 2003, Lovejoy *et al.* 2004) yielded thermochemical data for some of the reactions of hydrated $(HSO_4^-)_x \cdot (H_2SO_4)_y$ ions, which are very likely to play a significant role in the ion-induced nucleation mechanisms. Cluster properties predicted by bulk thermodynamics are not valid during the atmospheric nucleation processes. So far, conclusions on whether or not certain substances cause nucleation in the atmosphere are usually based on predictions given by the classical nucleation theory. Therefore, quantum chemical studies are needed to find reliable formation pathways for small clusters.

As shown for example by Nadykto *et al.* (2006), quantum chemical methods are able to explain qualitative or even quantitative features of ion-induced nucleation processes which are not well described by classical methods. As a first step in the computational investigation of ion-induced nucleation in the sulfuric acid–water system, we studied the hydration thermodynamics of the hydrogensulfate ion (HSO_4^-) and compared it to that of the neutral sulfuric acid molecule (H_2SO_4). We also studied the binding of ammonia to the hydrogensulfate ion in order to assess the possible role of ammonia in negative ion-induced nucleation.

Computational details

Our calculations were performed with the Gaussian 03 program suite (Frisch *et al.* 2004) using second- and fourth-order Møller-Plesset perturbation theory; MP2 (Møller and Plesset 1934) and MP4 (Krishnan and Pople 1978). The basis sets employed were the augmented correlation-consistent polarized split-valence sets aug-cc-pV($D + d$)Z and aug-cc-pV($T + d$)Z (Dunning 2001), which are improved version of the standard aug-cc-pVDZ and aug-cc-pVTZ sets (Dunning 1989, Wilson *et al.* 1996), and have been shown (Wang and Wilson 2004, Wilson and Dunning 2004) to produce more accurate results for sulfur-containing molecules. Our previous error analysis study (Kurtén *et al.* 2006) showed that these corrected, augmented correlation-consistent basis sets describe hydrogen-bonded clusters well.

For all species, several guess geometries were first optimized at the MP2/aug-cc-pV($D + d$)Z level. For the minimum energy structure, and all metastable isomers within 2 kcal mol⁻¹ of the minimum, we then carried out a frequency calculation at the MP2/aug-cc-pV($D + d$)Z level. Next, we carried out two higher-level single-point calculations on all isomers with a Gibbs free energy within 2 kcal/mol of the minimum structure: one at the MP2/aug-cc-pV($T + d$)Z and another at the MP4/aug-cc-pV($D + d$)Z level. For the neutral species, guess geometries were mainly obtained from earlier studies (Bandy and Ianni 1998, Re *et al.* 1999, Ding *et al.* 2003a). For the smallest ionic cluster $HSO_4^- \cdot (H_2O)$, the HF/6-31+G(d) structures of Froyd and Lovejoy (2003) were

used as input structures, while for the larger clusters, guess geometries were obtained by a combination of molecular dynamics simulations (using the potential developed by Ding *et al.* 2003b) and low-level (B3LYP/6-31++$G(d,p)$ with loose convergence criteria) quantum chemical optimizations.

The Gaussian default convergence criteria (listed in the Appendix) were used for the geometry optimizations and harmonic frequency calculations. For the anharmonic vibrational frequency calculations, tighter criteria of 10^{-5} a.u. and 1.5×10^{-5} a.u. with respect to the RMS and maximum forces, respectively, were used. The perturbative method with which the anharmonic vibrational frequencies were calculated is described by Barone (2005). All molecular structure figures were created using the MOLEKEL program (Portmann 2002).

Results and discussion

Method validation

Most previous studies on sulfuric acid–water clusters (Bandy and Ianni 1998, Re *et al.* 1999, Ding *et al.* 2003a, al Natsheh *et al.* 2004) were based on the density functional theory (DFT) methods. While DFT methods are computationally effective, and have been hugely successful in many quantum chemical applications, they have so far been unable to describe dispersive interactions (caused by non-local correlation) which play a moderately important role in hydrogen bonding. Recently, heavily parametrized functionals have been developed (*see* e.g. Zhao and Truhlar 2004, 2005) which reproduce well the experimentally determined binding energies and geometries for hydrogen-bonded species of some reference dataset. It should, however, be noted that the good agreement is achieved by parameter fitting instead of a fundamentally accurate physical description of the system. While these functionals probably represent the best alternative for computations on larger systems, correlated wave-function based methods are still the most systematically reliable tools for investigating weakly bound systems, especially those including bonding patterns not

present in the datasets used to build or test the functionals. Functionals containing explicit dispersion contributions are being developed (*see* e.g. Schwabe and Grimme 2006) but they are not yet generally available.

As the focus of this study is on obtaining accurate thermochemical results for relatively small clusters, we decided to use Møller-Plesset perturbation theory (MPn), which is known to describe hydrogen-bonded systems well. However, the use of MPn methods is challenging in three ways. First, the computational effort is significant, as even the MP2 method scales as roughly the fifth power of the system size (while DFT methods scale as the third or fourth power). Second, the MP methods converge much slower with respect to the basis set than do DFT methods. This is apparent for example in the basis-set superposition errors (BSSE) calculated in our earlier error analysis study (Kurtén *et al.* 2006). For the $H_2SO_4 \bullet H_2O$ cluster and the large aug-cc-pV($T + d$)Z basis set, the DFT methods B3LYP and PW91 yielded BSSE errors of less than 0.2 kcal mol^{-1}, while the BSSE error at the MP2 level was over 1 kcal mol^{-1}. However, this large value may be an overestimation, since the counterpoise correction (Boys and Bernardi 1970) used to evaluate BSSE errors often yields incorrect results for basis sets including multiple diffuse functions (Feller 1992). Third, the harmonic vibrational frequencies predicted by the MP2 method are usually (Foresman and Frisch 1996) further from the experimental (anharmonic) frequencies, resulting in larger errors if anharmonicity is neglected. Furthermore, it should be noted that as the MP2 method only recovers part of the correlation energy, higher-level corrections at even more prohibitively expensive levels (for example MP4, which scales formally as the seventh power of the system size) are required for accurate results.

In order to obtain accurate thermochemical parameters with a feasible computational effort, we clearly require some sort of multistep method: a scheme in which the geometry and vibrational frequencies are calculated at a lower level, after which various corrections to the binding energy — for example with respect to the basis set or the level of electron correlation — are then computed at this geometry. Vari-

ous well-established multistep methods already exist, such as the Gn family, but they are not well suited to weakly bound complexes as the basis sets employed in them contain few diffuse functions. For example, the G2 method (Curtiss *et al.* 1991) uses no diffuse functions in the geometry optimization, and only one set of diffuse functions on non-hydrogen atoms in the calculation of higher-level corrections. Diffuse functions on hydrogen atoms are not included at all.

In this study, we adapted the philosophy of established multistep methods to the aug-cc-pV($X + d$)Z basis sets, which we have shown (Kurtén *et al.* 2006) to be more suitable for the study of sulfuric acid–water clusters. After the initial MP2/aug-cc-pV($D + d$)Z optimization and frequency calculations, two higher-level corrections were calculated: the MP2/aug-cc-pV($T + d$)Z energy to account for basis-set effects beyond the double-zeta level, and the MP4/aug-cc-pV($D + d$)Z energy to account for electron correlation beyond the MP2 level. From the two MP2 energies, the basis-set limit energy could be extrapolated using the formula (Helgaker *et al.* 1997):

$$E(X) = E(\infty) + AX^{-3} \qquad (1)$$

where $E(\infty)$ is the basis-set limit energy, A is a constant, $X = 2$ for the aug-cc-pV($D + d$)Z set and $X = 3$ for the aug-cc-pV($T + d$)Z set. The purpose of the extrapolation is to remove not only basis-set superposition errors but also basis-set incompleteness errors, and thus provide a more reliable estimate of the basis-set limit than that given e.g. by the counterpoise correction (Boys and Bernadi 1970) (*see* the Appendix for test calculations of basis set dependencies on MP2 energies). The MP2 and MP4 energies can then be combined as follows:

$$
\begin{aligned}
E_{\text{3-step}} = &\, E\big[\text{MP2 /aug-}\infty Z\big] \\
&+ \big(E\big[\text{MP4 /aug-DZ}\big] \qquad (2) \\
&- E\big[\text{MP2 /aug-DZ}\big]\big)
\end{aligned}
$$

Were aug-[D or ∞]Z is an abbreviation of aug-cc-pV($X + d$)Z and the difference in parentheses in the right-hand side of the expression accounts for the higher-order correlation.

We tested the validity of our method with a series of test calculations on the smallest clus-

ters structures in our study: $H_2SO_4 \bullet H_2O$ and $HSO_4^- \bullet H_2O$. We optimized the geometry of these smallest clusters at the MP2/aug-cc-pV($T + d$)Z level, and also calculated electronic energies at the computationally very demanding MP4/aug-cc-pV($T + d$)Z level. The results are presented in appendix, and show that the combination of MP2/aug-cc-pV($D + d$)Z geometries with MP2/aug-cc-pV($T + d$)Z and MP4/aug-cc-pV($D + d$)Z single-point energies provide a relatively cost-effective way of calculating very accurate binding energies. We further carried out anharmonic frequency calculations at the MP2/aug-cc-pV($D + d$)Z level on the H_2O, H_2SO_4, HSO_4^-, $H_2SO_4 \bullet H_2O$, $HSO_4^- \bullet H_2O$ (two isomers), $H_2SO_4 \bullet (H_2O)_2$ and $HSO_4^- \bullet (H_2O)_2$ (two isomers) systems. The resulting vibrational frequencies and anharmonicity constants were used to determine two sets of scaling factors for the neutral clusters. The sf1 scaling factor set was used to fit the harmonic enthalpy and entropy contributions to the corresponding anharmonic ones calculated by using the anharmonic fundamental vibrational frequencies in the expressions derived for harmonic oscillators (a SPT model by Truhlar and Isaacson 1991, Barone 2004). The sf2 set was used to fit the harmonic enthalpy and entropy contributions to the corresponding anharmonic ones calculated using more accurate expressions involving the anharmonicity constants. For the hydrogensulfate ion, scaling factors could not be determined as one of its anharmonic vibrational frequencies was negative. Further test calculations revealed that this was caused by an internal rotation, which the perturbative anharmonic vibrational method was unable to treat properly. The anharmonic thermochemical parameters for HSO_4^- were determined by treating its lowest vibrational mode as a hindered internal rotation, and using the computed anharmonicity constants to calculate thermochemical contributions for the other modes. One of the $HSO_4^- \bullet H_2O$ isomers also appeared to posess an internal rotation, which caused one of the anharmonic overtone frequencies to be negative. This was also accounted for by treating the mode as a hindered internal rotation. The process is described in greater detail in the appendix. The sf2 and sf1 scaling factor sets for the larger clusters were determined by fitting to the anharmonic values of the dihydrate
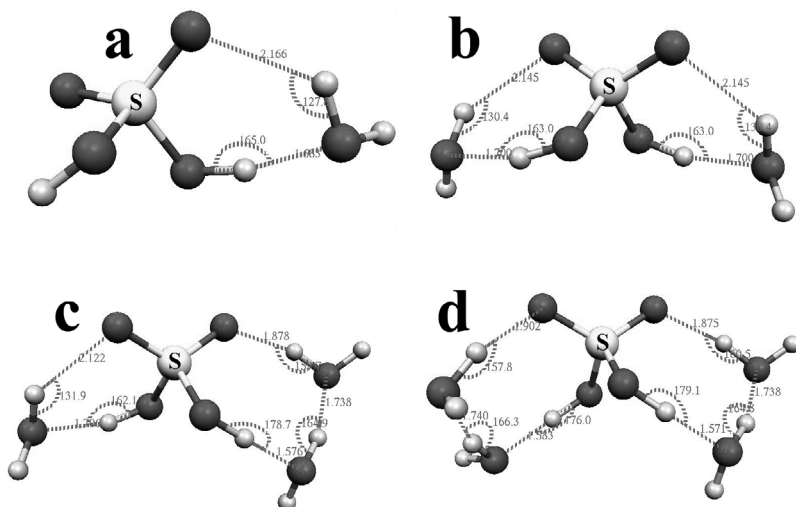
Fig. 1. Structure of the most stable neutral clusters:
(a) H$_2$SO$_4$•H$_2$O,
(b) H$_2$SO$_4$•(H$_2$O)$_2$,
(c) H$_2$SO$_4$•(H$_2$O)$_3$,
(d) H$_2$SO$_4$•(H$_2$O)$_4$.
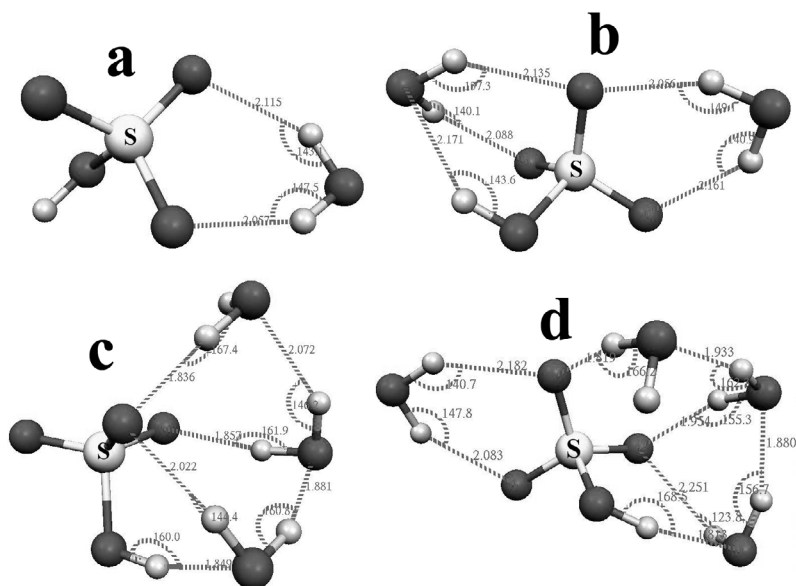
Fig. 2. Structure of the most stable anionic clusters:
(a) HSO$_4^-$•H$_2$O,
(b) HSO$_4^-$•(H$_2$O)$_2$,
(c) HSO$_4^-$•(H$_2$O)$_3$,
(d) HSO$_4^-$•(H$_2$O)$_4$.

structures HSO$_4^-$•(H$_2$O)$_2$ and H$_2$SO$_4$•(H$_2$O)$_2$ (*see* Appendix for details).

Comparison of neutral and ion clusters

The structure of the most stable neutral cluster structures (with respect to the Gibbs free energy of formation, calculated using the harmonic approximation, at 298 K) H$_2$SO$_4$•(H$_2$O)$_n$ with *n* = 1–4 is shown in Fig. 1 (cartesian co-ordinates of these structures, along with several metastable isomers, are given at http://www.borenv.net/

BER/pdfs/ber12/KurtenS1.pdf). The structures are qualitatively similar to those obtained in earlier DFT studies (Bandy and Ianni 1998, Re *et al*. 1999). It should be noted that the high-level method employed here does not predict proton transfer to occur for the H$_2$SO$_4$•(H$_2$O)$_4$ cluster, unlike the B3LYP/6-311++G(2d,2p) study by Bandy and Ianni (1998). However, in both cases the energy difference between the most stable clusters with and without proton transfer is very small.

The structure of the most stable (with respect to the Gibbs free energy of formation, calculated

using the harmonic approximation, at 298 K) anionic cluster structures $HSO_4^- \bullet (H_2O)_n$ with n = 1–4 is shown in Fig. 2 (cartesian co-ordinates of these structures, along with several metastable isomers are given at http://www.borenv.net/BER/pdfs/ber12/KurtenS1.pdf). By comparing the structures of the neutral and anionic clusters (Figs. 1 and 2), it can be seen that the larger anionic clusters contain more hydrogen bonds than the corresponding neutral clusters. Presumably, the H-bonds are also stronger, as the hydrogen atoms of the water molecules are attracted toward the negatively charged core ion.

The electronic energies, enthalpies, entropies and Gibbs free energies computed for the water addition reaction to various clusters are listed in Tables 1 and 2. All the values refer to reactions between the most stable cluster structures (with respect to the Gibbs free energy, calculated using the harmonic approximation, at 298 K). More information on the calculated energies for both these and all studied metastable cluster structures is given at http://www.borenv.net/BER/pdfs/ber12/KurtenS2.pdf. Note that the most stable isomers with respect to the electronic energy and free energy are different for some cluster stoichiometries. The reaction energies at all three computed levels [MP2/aug-cc-pV($D + d$)Z, MP2/aug-cc-pV($T + d$)Z and MP4/aug-cc-pV($D + d$)Z] are presented in Table 1. 'ΔE_0, 3-step' corresponds to the combination of the fitted MP2/aug-cc-pV($\infty + d$)Z basis set limit with the MP2 – MP4 difference, as described in the section 'Method validation'. The parameters presented in Table 2 are calculated using the multistep electronic energies and the scaling

factor sets sf1 and sf2, described in detail in the Appendix.

The formation free energies for the $H_2SO_4 \bullet H_2O$ and $H_2SO_4 \bullet (H_2O)_2$ clusters are in excellent agreement with experimental results (*see* Hanson and Eisele 2000) when the anharmonic vibrational corrections are accounted for. For the ionic clusters, the reaction enthalpies and entropies for individual water addition reactions vary strongly, and the agreement with experimental results (Blades *et al.* 1995, Froyd and Lovejoy 2003) is not always good. However, the computed (anharmonic, using the sf2 scaling factor set) enthalpy and entropy changes for example for the cumulative reaction HSO_4^- + 4 H_2O => $HSO_4^- \bullet (H_2O)_4$ (–48.84 kcal mol^{-1} and –110.7 cal Kmol^{-1}, respectively) are very close to the corresponding experimental values (–49.7 kcal mol^{-1} and –112 cal Kmol^{-1}, respectively). This indicates that the differences observed for individual water addition reactions may be due to configurational sampling issues, such as the fact that only the most stable isomers (with repect to the free energy at 298 K) were used to calculate the reaction energetics shown here. As the experiments were performed at quite low temperatures of 221–271 K (the experimental 298 K values are extrapolations), it is quite possible that the experimental values contain significant contributions from some isomers which are less stable at 298 K (*see* http://www.borenv.net/BER/pdfs/ber12/KurtenS2.pdf). We tested the effect of including contributions from the metastable isomers to the computed enthalpies and entropies to give "ensemble-averaged" values. We also tested the effect of using the scaling factors obtained from

Table 1. Reaction energies computed for the water addition reactions at different levels. DZ and TZ correspond to aug-cc-pV($D + d$)Z and aug-cc-pV($T + d$)Z, respectively.

Reaction	ΔE_0, MP2/DZ (kcal mol^{-1})	ΔE_0, MP2/TZ (kcal mol^{-1})	ΔE_0, MP4/DZ (kcal mol^{-1})	ΔE_0, 3-step (kcal mol^{-1})
$H_2SO_4 + H_2O$ => $H_2SO_4 \bullet H_2O$	–12.73	–13.01	–12.74	–13.14
$H_2SO_4 \bullet H_2O + H_2O$ => $H_2SO_4 \bullet (H_2O)_2$	–12.63	–12.72	–12.71	–12.84
$H_2SO_4 \bullet (H_2O)_2 + H_2O$ => $H_2SO_4 \bullet (H_2O)_3$	–12.39	–12.65	–12.30	–12.66
$H_2SO_4 \bullet (H_2O)_3 + H_2O$ => $H_2SO_4 \bullet (H_2O)_4$	–13.12	–12.91	–13.09	–12.79
$HSO_4^- + H_2O$ => $HSO_4^- \bullet H_2O$	–14.77	–14.77	–15.00	–15.01
$HSO_4^- \bullet H_2O + H_2O$ => $HSO_4^- \bullet (H_2O)_2$	–16.48	–16.67	–16.71	–16.97
$HSO_4^- \bullet (H_2O)_2 + H_2O$ => $HSO_4^- \bullet (H_2O)_3$	–15.13	–14.88	–15.49	–15.13
$HSO_4^- \bullet (H_2O)_3 + H_2O$ => $HSO_4^- \bullet (H_2O)_4$	–10.89	–10.64	–11.09	–10.74

the more anharmonic $HSO_4^-•(H_2O)_2$ (ii) isomer to compute the thermochemical parameters for the larger clusters. The results (*see* Table A8 of the Appendix) indicate that including contributions from metastable isomers has a moderate effect on the thermochemical parameters. For the $HSO_4^- + H_2O => HSO_4^-•(H_2O)$, $HSO_4^-•(H_2O) + H_2O => HSO_4^-•(H_2O)_2$ and $HSO_4^-•(H_2O)_2 + H_2O => HSO_4^-•(H_2O)_3$ reactions, ensemble-averaging and using the more anharmonic scaling factor sets somewhat improves the agreement of computed and experimental enthaply and entropy

changes. However, for the $HSO_4^-•(H_2O)_3 + H_2O => HSO_4^-•(H_2O)_4$ reaction, all computed datasets are far from the experimental values. It is possible that this discrepancy is related to unidentified hindered rotations in the ionic tri- or tetrahydrates.

The fact that the cumulative reaction energetics agree, while the individual reaction energetics differ, might also indicate that there could be some uncertainty in the experimentally measured number of water molecules in a cluster. If this is the case, e.g. the data reported by Froyd and Lovejoy (2003) for two-water clusters could

Table 2. Reaction thermodynamics computed for water addition reactions at 298 K and a reference pressure of 1 atm.

Reaction	ΔS, 298K (cal Kmol^{-1})	ΔH, 298K (kcal mol^{-1})	ΔG, 298K (kcal mol^{-1})
$H_2SO_4 + H_2O => H_2SO_4•H_2O$	−29.15[a]	−11.50[a]	−2.81[a]
	−27.49[b]	−11.50[b]	−3.30[b]
	−25.76[c]	−11.12[c]	−3.44[c]
			−3.6 ± 1[d]
$H_2SO_4•H_2O + H_2O => H_2SO_4•(H_2O)_2$	−30.90[a]	−11.08[a]	−1.87[a]
	−29.33[b]	−11.10[b]	−2.35[b]
	−28.90[c]	−10.92[c]	−2.30[c]
			−2.30 ± 0.3[d]
$H_2SO_4•(H_2O)_2 + H_2O => H_2SO_4•(H_2O)_3$	−29.20[a]	−11.07[a]	−2.37[a]
	−28.11[b]	−11.07[b]	−2.69[b]
	−27.46[c]	−10.94[c]	−2.75[c]
$H_2SO_4•(H_2O)_3 + H_2O => H_2SO_4•(H_2O)_4$	−34.49[a]	−11.19[a]	−0.90[a]
	−33.43[b]	−11.18[b]	−1.21[b]
	−32.79[c]	−11.04[c]	−1.26[c]
$HSO_4^- + H_2O => HSO_4^-•H_2O$	−28.01[a]	−13.35[a]	−5.00[a]
	−24.32[b]	−13.47[b]	−6.22[b]
	−22.64[c]	−12.95[c]	−6.20[c]
	−23.00[e]	−12.90[e]	−5.90[f]
$HSO_4^-•H_2O + H_2O => HSO_4^-•(H_2O)_2$	−32.61[a]	−13.48[a]	−3.76[a]
	−32.44[b]	−13.11[b]	−3.44[b]
	−33.35[c]	−13.39[c]	−3.45[c]
	−22.0[e]	−11.20[e]	−4.70[f]
$HSO_4^-•(H_2O)_2 + H_2O => HSO_4^-•(H_2O)_3$	−39.83[a]	−12.90[a]	−1.03[a]
	−39.12[b]	−14.46[b]	−2.80[b]
	−38.95[c]	−14.39[c]	−2.78[c]
	−30.70[e]	−12.40[e]	
$HSO_4^-•(H_2O)_3 + H_2O => HSO_4^-•(H_2O)_4$	−25.13[a]	−9.30[a]	−1.81[a]
	−24.02[b]	−9.28[b]	−2.12[b]
	−23.76[c]	−9.22[c]	−2.14[c]
	−36.30[e]	−13.20[e]	

[a] Harmonic values, internal rotations are ignored. [b] Anharmonic values, using fundamental frequencies for the smaller clusters and the sf1 scaling factor set for clusters that contain more than two water molecules, accounting approximately for the identified internal rotations. [c] Anharmonic values, using anharmonicity constants for the smaller clusters and the sf2 scaling factor set for clusters that contain more than two water molecule, accounting approximately for the identified internal rotations. [d] Experimental values, Hanson and Eisele (2000). [e] Experimental values, Froyd and Lovejoy (2003). [f] Experimental values, Blades *et al.* (1995), at 293 K. All computed values correspond to the ΔE_0, 3-step electronic energies (Table 1).

contain some contributions from one- and three-water clusters.

A comparison of the electronic and Gibbs free energies for hydration reactions demonstrates that the hydrogensulfate ion binds water significantly more strongly than sulfuric acid. For the first two water addition reactions, the differences in electronic or free energies are around 1.5–2 kcal mol^{-1}, with the application of anharmonicity corrections tending to decrease the differences. For the third and fourth addition reactions, the difference decreases to below 1 kcal mol^{-1} as the additional water molecules are increasingly bound to other waters instead of to the core acid or ion. Presumably, the difference would decrease even further if more water molecules were added. However, as the degree of hydration in atmospheric conditions is mainly determined by the equilibrium constants of the first water addition reactions, we can conclude from the data that the hydrogensulfate ion will be much much more extensively hydrated than the neutral acid molecule.

Basis-set superposition errors have been evaluated for the two-molecule clusters using the counterpoise method (Boyd and Bernadi 1970). The results (*see* Table A4 of the Appendix) seem to indicate that the magnitude of the basis-set superposition errors for the dimer clusters at the MP2 level is around 2 kcal mol^{-1} for the aug-cc-pV(D + d)Z and 1 kcal mol^{-1} for the aug-cc-pV(T + d)Z basis sets. However, further test calculations (*see* Table A5) on larger basis sets up to aug-cc-pV(5 + d)Z quality show that the differences between aug-cc-pV(D + d)Z or aug-cc-pV(T + d)Z and basis set limit binding energies are likely to be almost an order of magnitude smaller than predicted by the counterpoise correction. This is probably related to the presence of multiple diffuse functions in the basis sets, as noted e.g. by Feller (1992). We also note that including the counterpoise corrections would significantly deteriorate the agreement between computed and experimental results for almost all clusters studied.

Sulfuric acid hydrate formation

In atmospheric studies of particle formation involving sulfuric acid, it is vital to know the ratio of free sulfuric acid molecules to the total number of sulfuric acid molecules (free molecules + those bound to small clusters). The total number is the measured sulfuric acid concentration, but the free number enters the calculation of formation free energy of the clusters, and thus also the exponential of this energy, which is the main factor determining the particle formation rate.

The equilibrium constants K_i for hydrate formation are defined as

$$
\begin{aligned}
K_i &= \frac{\left(\rho_{\text{aiw}}/\rho_0\right)}{\left(\rho_{\text{w}}/\rho_0\right)\left(\rho_{\text{a(i-1)w}}/\rho_0\right)}, \\
&= \exp\left[-\frac{(\Delta H_{\text{aiw}} - T\Delta S_{\text{aiw}})}{RT}\right]
\end{aligned}
\tag{3}
$$

where ρ_{aiw} is the concentration of hydrates with one acid and i water molecules, ρ_{w} is the concentration of water molecules, ρ_0 is the reference vapor concentration ($\rho_0 = 1$ atm/$(k_{\text{b}}T)$), k_{b} is Boltzmann's constant, R is the molar gas constant, and ΔH_{aiw} and ΔS_{aiw} are the standard reaction enthalpy and entropy per mole for a reaction where a i-hydrate is formed from a ($i - 1$)-hydrate and a water molecule. In the atmosphere, where the concentration of water is much higher than the concentration of sulfuric acid, hydrate formation does not cause the free water molecule concentration to deviate significantly from the total water concentration. The ratio of total to free number of acid molecules is given by

$$
\begin{aligned}
\frac{\rho_{\text{a}}^{\text{total}}}{\rho_{\text{a}}^{\text{free}}} &= 1 + K_1\frac{\rho_{\text{w}}}{\rho_0} + K_1 K_2\left(\frac{\rho_{\text{w}}}{\rho_0}\right)^2 \\
&\quad + \ldots + K_1 K_2 \ldots K_4\left(\frac{\rho_{\text{w}}}{\rho_0}\right)^4
\end{aligned}
\tag{4}
$$

It can be seen from Fig. 3 that to get agreement with experiments, we have to select the most accurate treatment possible. Both basis-set effects, higher-order correlation and anharmonicity must be accounted for in order to quantitatively match quantum chemical results with experiments. It should be noted that though the predicted free to total ratios are still slightly higher than the experimental ones, our predictions are well within the experimental error limits.

The present hydrate model used in atmospheric applications (Noppel *et al.* 2002) is partly based on the classical liquid drop model, partly on quantum chemistry, the combination of
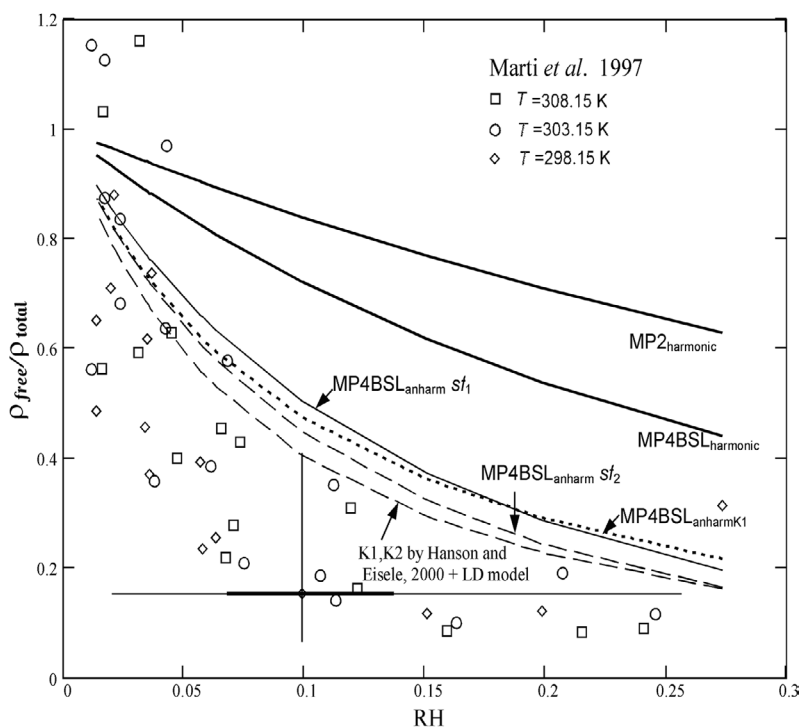
Fig. 3. Comparison of *ab initio* hydration results with experimental data by Marti *et al.* (1997) at *T* = 298.15 K. The large cross characterizes the uncertainty of experimental data (Marti *et al.* estimated the composition uncertainty of solutions in their experiments to be 15% and the uncertainty of obtained total vapor pressures of acid to be 36%. The uncertainty of pure vapor pressure of acid by Ayers *et al.* (1980) is also included. The thick part of the cross corresponds to the uncertainty of mass fraction of acid ± 0.028 estimated by the scattering of data points (Noppel *et al.* 2002). RH is the relative humidity in the saturated vapor above an aqueous solutions of sulfuric acid. MP2$_{harmonic}$ corresponds to MP2/aug-cc-pV(D + d)Z electronic energies, with free energies computed using the harmonic oscillator and rigid rotor approximations. MP4BSL$_{harmonic}$ corresponds to the three-step electronic energies described in this article (with basis-set limit and MP4 corrections), with free energies computed using the harmonic oscillator and rigid rotor approximations. MP4BSL$_{anharm}$ sf$_1$ and MP4BSL$_{anharm}$ sf$_2$ contain anharmonic corrections computed using the sf1 and sf2 scaling factor sets, respectively (*see* the article text and appendix for details). MP4BSL$_{anharmK1}$ has been computed by combining the anharmonic formation free energy for the acid monomer with the harmonic formation free energies of the dimer, trimer and tetramer. We also show the free to total acid ratio calculated using the experimental equilibrium contants of Hanson and Eisele (2000) for mono-and dihydrate formation (K_1 and K_2), and classical liquid drop model for the hydrates with 3–5 water molecules.

which has been fitted to yield the experimental results (shown in Fig. 3). In the view of large experimental uncertainties and the accuracy of the quantum chemical results of this study, we present here a solely quantum chemistry-based hydration model using the computational results that match the experiments most closely.

Below we present polynomial fits for the temperature dependence of the reaction entropies and enthalpies in the range of 140 K < *T* < 400 K. The accuracy is 0.2% for the enthalpies, 0.3% for the entropies, and 3% for the equilibrium constants. The temperature *T* in the fol-

lowing equations is given in Kelvin. The fits are based on the 3-step electronic energies presented above, with anharmonicity taken into account by using the scaling factor set sf2.

$$\Delta H_{a1w}(T)/(R \times K) = -5640.7 - 2.714T$$
$$+ 0.01119T^2 - 5.348 \times 10^{-6}T^3$$
$$\Delta H_{a2w}(T)/(R \times K) = -5456 - 1.976T$$
$$+ 0.006128T^2 \qquad (5)$$
$$\Delta H_{a3w}(T)/(R \times K) = -5603 + 1.391T$$
$$- 0.003662T^2$$
$$\Delta H_{a4w}(T)/(R \times K) = -5331 - 1.647T$$
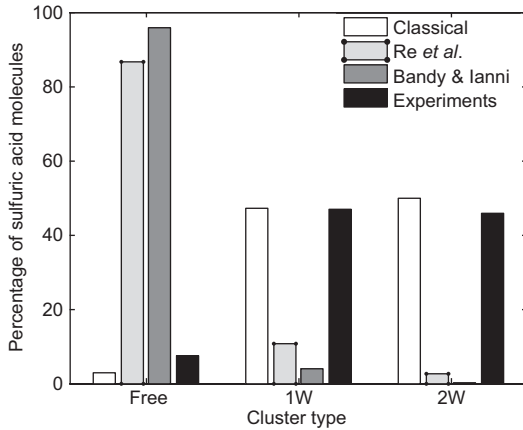$$+ 0.003766T^2$$

Fig. 4. Hydrate distribution of neutral sulfuric acid at 298 K and RH = 50% as predicted by the earlier quantum chemical studies of Re *et al.* (1999), Bandy and Ianni (1998), the experimental study of Hanson and Eisele (2000), and the classical model of Noppel *et al.* (2002). The *y*-axis is the relative fraction of sulfuric acid molecules bound to each type of cluster, and the *x*-axis indicates the number of water molecules bound to the cluster. "Free" corresponds to the unhydrated acid.

$$\Delta S_{a1w}(T)/R = -13.34 - 0.01104T + 5.784$$
$$\times 10^{-5}T^2 - 5.556 \times 10^{-8}T^3$$
$$\Delta S_{a2w}(T)/R = -14.79 - 0.003969T$$
$$+ 1.572 \times 10^{-5}T^2 \qquad (6)$$
$$\Delta S_{a3w}(T)/R = -13.55 + 9.039 \ 10^{-4}T$$
$$- 8.041 \times 10^{-6}T^2$$
$$\Delta S_{a4w}(T)/R = -15.32 - 0.008266T$$
$$+ 1.580 \times 10^{-5}T^2$$

For the $H_2SO_4 \bullet (H_2O)_3$ cluster, the most stable structures with respect to the electronic energy and the Gibbs free energy at 298 K were different. Hence, contributions from both isomers are included in Eqs. 5 and 6 (*see also* http://www.borenv.net/BER/pdfs/ber12/KurtenS2.pdf). As the combinatorial nature of the configurational sampling problem makes it almost certain that all minimum geometries have not been sampled at least for the larger cluster structures, no other metastable isomers were included in the calculations.

Comparison of neutral and ion hydrate formation

Hydrate distributions derived from earlier quan-

tum chemical studies were in strong disagreement with Hanson and Eisele (2000) experimental data (Fig. 4).

The hydrate distributions (at 298 K and three relative humidities) for the neutral sulfuric acid and hydrogensulfate ion computed from the data in this study are shown in Figs. 5 and 6. The distributions were computed using the anharmonic (sf2 scaling factor set) formation enthalpies and entropies with Eq 3. Relative humidities were converted into water partial pressures with the formula given by Seinfeld and Pandis (1998). The results show that, as expected from the thermodynamic data, the hydrogensulfate ion is more extensively hydrated than neutral sulfuric acid in all conditions. While a significant percentage of the neutral sulfuric acid remains unhydrated at RH 20% and 50%, the fraction of unhydrated hydrogensulfate ions is negligible in all studied conditions. For the neutral acid, the peak of the hydrate distribution is located at 1 water molecule for RH 20%, approximately 2 water molecules for RH 50% and 3 water molecules for RH 80%. For the hydrogensulfate ion, the peak is located at 3 water molecules for RH 20% and 50%, and at 4 water molecules or possibly more for RH 80%.

Test calculations were carried out to investigate the temperature and RH data ranges for which truncation of the dataset at 4 water molecules is likely to significantly affect the predicted total degree of hydration. If a limit of 20% for the relative concentration of the four-water clusters is taken as a indication of possibly significant truncation errors, the neutral sulfuric acid hydrate distribution is unlikely to be affected at any temperature as long as the RH does not significantly exceed 100% (e.g. at 298 K, a RH of 130% is required for the limit to be reached). This confirms the assumption, made in the previous section, that neutral hydrates with more than 4 water molecules do not affect the free to total acid ratio significantly. However, for the ionic hydrate distribution the situation is very different. The limit of 20% concentration for the $HSO_4^- \bullet (H_2O)_4$ cluster is reached already at RH 40% at a temperature of 298 K. Decreasing the temperature raises the limiting RH value, but quite slowly, e.g. at 240 K it is still only 50% (the reason for the small change is that the
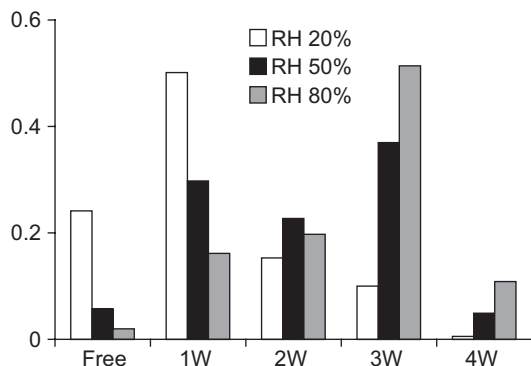
Fig. 5. Hydrate distribution of neutral sulfuric acid at 298 K and three different relative humidities. The *y*-axis is the relative fraction of sulfuric acid molecules bound to each type of cluster, and the *x*-axis indicates the number of water molecules bound to the cluster. "Free" corresponds to the unhydrated acid.
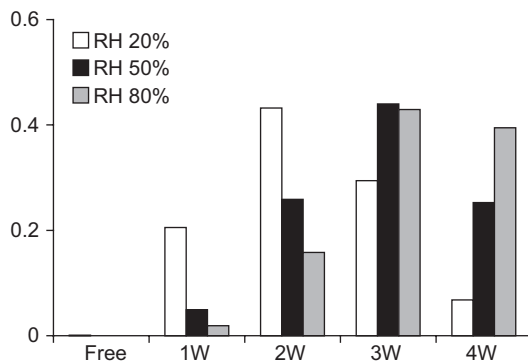

Fig. 6. Hydrate distribution of the hydrogensulfate ion at 298 K and three different relative humidities. The *y*-axis is the relative fraction of ions bound to each type of cluster, and the *x*-axis indicates the number of water molecules bound to the cluster. "Free" corresponds to the unhydrated ion.

strong temperature dependencies of the hydrate formation free energies and the saturation vapour pressure of water mostly cancel out each other). We can thus conclude that modelling the full hydration of the HSO_4^- ion at all atmospheric conditions would require the addition of several more water molecules to the dataset.

Assessing the role of ammonia in ion-induced nucleation

Finally, we calculated the formation energies, enthalpies, entropies and Gibbs free energies for the $H_2SO_4 \bullet NH_3$, $(HSO_4^-) \bullet NH_3$, $H_2SO_4 \bullet NH_3 \bullet H_2O$ and $(HSO_4^-) \bullet NH_3 \bullet H_2O$ clusters (only harmonic thermochemical parameters are shown as the comparison is intended to be qualitative in nature, and no scaling factors were determined for ammonia-containing clusters). The most stable cluster structures are shown in Fig.

7. The neutral clusters structures are similar to those presented by Ianni and Bandy (1998). Our results (*see* Tables 3 and 4) show that ammonia is much more strongly bonded to the neutral acid molecule than to the hydrogensulfate ion. Indeed, the binding of ammonia to HSO_4^- is predicted to be weakly endothermic at 298 K. The reason for the large difference in the binding energies is probably the fact that H_2SO_4 is a strong acid, and thus highly attracted to ammonia (which is a moderately strong base), while HSO_4^- is a very weak acid, and therefore less attracted to the basic ammonia molecule. Additionally, a comparison of the results for the ammonia-containing and ammonia-free clusters (Tables 1–2 and 3–4, respectively) shows that the presence of ammonia does not increase the affinity of the HSO_4^- toward water. These results imply that ammonia will probably not enhance ion-induced nucleation in the sulfuric acid-water system like it does for neutral nucleation. However, further

Table 3. Reaction energies for ammonia-contaning clusters computed at different levels. DZ and TZ correspond to aug-cc-pV(*D* + *d*)*Z* and aug-cc-pV(*T* + *d*)*Z*, respectively.

Reaction	ΔE_0, MP2/DZ (kcal mol⁻¹)	ΔE_0, MP2/TZ (kcal mol⁻¹)	ΔE_0, MP4/DZ (kcal mol⁻¹)	ΔE_0, 3-step (kcal mol⁻¹)
$H_2SO_4 + NH_3 => H_2SO_4 \bullet NH_3$	−16.99	−17.08	−16.59	−16.72
$H_2SO_4 \bullet NH_3 + H_2O => H_2SO_4 \bullet NH_3 \bullet H_2O$	−12.10	−12.32	−12.20	−12.51
$HSO_4^- + NH_3 => HSO_4^- \bullet NH_3$	−10.78	−10.59	−10.99	−10.71
$HSO_4^- \bullet NH_3 + H_2O => HSO_4^- \bullet NH_3 \bullet H_2O$	−14.63	−14.70	−14.73	−14.84

Fig. 7. Structure of the most stable ammonia-containing clusters:
(**a**) $H_2SO_4 \cdot NH_3$,
(**b**) $H_2SO_4 \cdot NH_3 \cdot H_2O$,
(**c**) $HSO_4^- \cdot NH_3$,
(**d**) $HSO_4^- \cdot NH_3 \cdot H_2O$.

Table 4. Reaction thermodynamics computed for water addition reactions to ammonia-containing clusters at 298 K and a reference pressure of 1 atm.

Reaction	ΔS	ΔH	ΔG
$H_2SO_4 + NH_3 => H_2SO_4 \cdot NH_3$	−27.68	−15.28	−7.16
$H_2SO_4 \cdot NH_3 + H_2O => H_2SO_4 \cdot NH_3 \cdot H_2O$	−30.69	−10.44	−1.60
$HSO_4^- + NH_3 => HSO_4^- \cdot NH_3$	−32.37	−9.24	+0.69
$HSO_4^- \cdot NH_3 + H_2O => HSO_4^- \cdot NH_3 \cdot H_2O$	−30.00	−13.07	−4.23

calculations on larger clusters containing neutral sulfuric acid and additional water molecules in addition to the HSO_4^- core ion will be required to conclusively settle this issue.

Conclusions

We computed formation energies for clusters containing one sulfuric acid molecule or hydrogensulfate ion and up to four water or one ammonia and one water molecules. The results demonstrate that the hydrogensulfate ion is bonded much more strongly to water than the neutral sulfuric acid molecule, and is hence expected to be more extensively hydrated in atmospheric conditions. This study represents the first high-level quantum chemical study of ion-induced nucleation of the hydrogensulfate core ion. In contrast to previous, lower level studies, the quantum chemical data presented here replicate the experimentally observed free to total acid ratio for hydrated sulfuric acid. A comparison of ammonia-containing clusters indicates that ammonia might not play any role in ion-induced nucleation involving the

hydrogensulfate core ion. However, further calculations on larger clusters are needed to determine whether or not this is the case.

References

Al Natsheh A., Nadykto A.B., Mikkelsen K.V., Yu F. & Ruuskanen J. 2004. Sulfuric acid and sulfuric acid hydrates in the gas phase: a DFT investigation. *J. Phys. Chem. A* 108: 8914–8929.

Anttila T., Vehkamäki H., Napaeri I. & Kulmala M. 2005. Effect of ammonium bisulphate formation on atmospheric water-sulphuric acid-ammonia nucleation. *Boreal Env. Res.* 10: 511–523.

Ayers G.P., Gillett R.W. & Gras J.L. 1980. On the vapor pressure of sulfuric acid. *Geophys. Res. Lett.* 7: 433–436.

Bandy A.R. & Ianni J.C. 1998. Study of hydrates of H_2SO_4 using density functional theory. *J. Phys. Chem. A* 102: 6533–6539.

Barone V. 2004. Vibrational zero-point energies and functions beyond the harmonic approximation. *J. Chem. Phys.* 120: 3059–3065.

Barone V. 2005. Anharmonic vibrational properties by a fully automated second-order perturbative approach. *J. Chem. Phys.* 122, 014108.

Bernd T., Böge O., Stratmann F., Heintzenberg J. & Kulmala M. 2005. Rapid formation of new sulfuric acid particles at near-atmospheric conditions. *Science* 307: 698–700.

Blades A.T., Klassen J.S. & Kebarle P. 1995. Free energies of hydration in the gas phase of anions of some oxo acids of C, N, S, P, Cl and I. *J. Am. Chem. Soc.* 117: 10563–10571.

Boys S.F. & Bernardi F. 1970. The calculation of small molecular interactions by the differences of separate total energies. *Mol. Phys.* 19: 553.

Couling S.B., Sully K.J. & Horn A.B. 2003a. Experimental study of the heterogeneous interaction of SO_3 and H_2O: formation of condensed phase molecular sulfuric acid hydrates. *J. Am. Chem. Soc.* 125: 1994–2003.

Couling S.B., Fletcher J., Horn A.B., Newnham D.A., McPheat R.A. & Williams R.G. 2003b. First detection of molecular hydrate complexes in sulfuric acid aerosols. *Phys. Chem. Chem. Phys.* 5: 4108–4113.

Curtiss L.A., Raghavachari K., Trucks G.W. & Pople J.A. 1991. Gaussian-2 theory for molecular energies of first- and second-row compounds. *J. Chem. Phys.* 94: 7221–7230.

Ding C.-G., Laasonen K. & Laaksonen A. 2003a. Two sulfuric acids in small water clusters. *J. Phys. Chem. A* 107: 8648–8658.

Ding C.-G., Taskila T., Laasonen K. & Laaksonen A. 2003b. Reliable potential for small sulfuric acid-water clusters. *Chem. Phys.* 287: 7–19.

Dunning T.H.Jr. 1989. Gaussian basis sets for use in correlated molecular calculations. I. The atoms boron through neon and hydrogen. *J. Chem. Phys.* 90: 1007–1023.

Dunning T.H.Jr., Peterson K.A. & Wang A.K. 2001. Gaussian basis sets for use in correlated molecular calculations. X. The atoms aluminum through argon revisited. *J. Chem. Phys.* 114: 9244–9253.

Feller A.D. 1992. Application of systematic sequences of wave functions to the water dimer. *J. Chem. Phys.* 96: 6104–6114.

Foresman J.B. & Frisch Æ. 1996. *Exploring chemistry with electronic structure methods*, 2nd ed. Gaussian, Inc., Wallingford CT.

Frisch M.J., Trucks G.W., Schlegel H.B., Scuseria G.E., Robb M.A., Cheeseman J.R., Montgomery J.A.Jr., Vreven T., Kudin K.N., Burant J.C., Millam J.M., Iyengar S.S., Tomasi J., Barone V., Mennucci B., Cossi M., Scalmani G., Rega N., Petersson G.A., Nakatsuji H., Hada M., Ehara M., Toyota K., Fukuda R., Hasegawa J., Ishida M., Nakajima T., Honda Y., Kitao O., Nakai H., Klene M., Li X., Knox J.E., Hratchian H.P., Cross J.B., Bakken V., Adamo C., Jaramillo J., Gomperts R., Stratmann R.E., Yazyev O., Austin A.J., Cammi R., Pomelli C., Ochterski J.W., Ayala P.Y., Morokuma K., Voth G.A., Salvador P., Dannenberg J.J., Zakrzewski V.G., Dapprich S., Daniels A.D., Strain M.C., Farkas O., Malick D.K., Rabuck A.D., Raghavachari K., Foresman J.B., Ortiz J.V., Cui Q., Baboul A.G., Clifford S., Cioslowski J., Stefanov B.B., Liu G., Liashenko A., Piskorz P., Komaromi I., Martin R.L., Fox D.J., Keith T., Al-Laham M.A., Peng C.Y., Nanayakkara A., Challacombe M., Gill P.M.W., Johnson B., Chen W., Wong M.W., Gonzalez C. & Pople J.A. 2004. *Gaussian 03, revision C.02.* Gaussian, Inc., Wallingford CT.

Froyd K.D. & Lovejoy E.R. 2003. Experimental thermodynamics of cluster ions composed of H_2SO_4 and H_2O. 2. Measurements and *ab initio* structures of negative ions. *J. Phys. Chem. A* 107: 9812–9824.

Hanson D.R. & Eisele F.L. 2000. Diffusion of H_2SO_4 in humidified nitrogen: hydrated H_2SO_4. *J. Phys. Chem. A* 104: 1715–1719.

Helgaker T., Klopper W., Koch H. & Noga J. 1997. Basisset convergence of correlated calculations on water. *J. Chem. Phys.* 106: 9639–9646.

Ianni J.C. & Bandy 1999. A density functional theory study of the hydrates of $NH_3 \bullet H_2SO_4$ and its implications for the formation of new atmospheric particles. *J. Phys. Chem A.* 103: 2801–2811.

Kulmala M., Pirjola L. & Mäkelä J. M. 2000 Stable sulphate clusters as a source of new atmospheric particles. *Nature* 404: 66–69.

Kulmala M. 2003 How particles nucleate and grow. *Science* 302: 1000–1001.

Kulmala M., Vehkamäki H., Petäjä T., Dal Maso M., Lauri A., Kerminen V.-M., Birmili W. & McMurry P.H. 2004. Formation and growth rates of ultrafine atmospheric particles: a review of observations. *J. Aerosol Sci.* 35: 143–176.

Kulmala M., Lehtinen K.E.J. & Laaksonen A. 2006. Cluster activation theory as an explanation of the linear dependence between formation rate of 3 nm particles and sulphuric acid concentration. *Atmos. Chem. Phys.* 6: 787–793.

Kurtén T., Sundberg M., Vehkamäki H., Noppel M., Blomqvist J. & Kulmala M. 2006. An *ab initio* and density functional theory reinvestigation of gas-phase sulfuric acid monohydrate and ammonium hydrogensulfate. *J. Phys. Chem. A* 110: 7178–7188.

Krishnan R. & Pople J.A. 1978. Approximate fourth-order perturbation theory of the electron correlation energy. *Int. J. Quant. Chem.* 14: 91–100.

Laakso L., Gagné S., Petäjä T., Hirsikko A., Aalto P.P., Kulmala M. & Kerminen V.-M. 2006. Detecting charging state of ultra-fine particles: instrumental development and ambient measurements. *Atmos. Chem. Phys. Discuss.* 6: 6401–6429.

Lee S.-H., Reeves J.M., Wilson J.C., Hunton D.E., Viggiano A.A., Miller T.M., Ballenthin J.O. & Lait L.R. 2003. Particle formation by ion nucleation in the upper troposphere and lower stratosphere. *Science* 301: 1886–1889.

Lovejoy E.R., Curtius J. & Froyd K.D. 2004. Atmospheric ion-induced nucleation of sulfuric acid and water. *J. Geophys. Res.* 109, D08204.

Marti J.J., Jefferson A., Cai X.P., Richert C., McMurry P.H. & Eisele F. 1997. H_2SO_4 vapor pressure of sulfuric acid and ammonium sulfate solutions. *J. Geophys. Res.* 102: 3725–3735.

Møller C. & Plesset M.S. 1934. Note on an approximation treatment for many-electron systems. *Phys. Rev.* 46: 618–622.

Nadykto A.B., Al Natsheh A., Yu F., Mikkelsen K.V. & Ruuskanen J. 2006. Quantum nature of the sign Preference in Ion-Induced Nucleation. *Phys. Rev. Lett.* 96, 125701.

Noppel M., Vehkamäki H. & Kulmala M. 2002. An improved model for hydrate formation in sulfuric acid-water nucleation. *J. Chem. Phys.* 116: 218–228.

O'Dowd C.D., Jimenez J.L., Bahreini R., Flagan R.C., Seinfeld J.H., Hämeri K., Pirjola L., Kulmala M., Jennings S.G. & Hoffmann T. 2002. Marine aerosol formation from biogenic iodide emissions. *Nature* 417: 632–636.

Portmann S. 2002. *MOLEKEL, version 4.3. win32*. Centro Svizzero di Calcolo Scientifico (CSCS)/ETHZ, Switzerland.

Re S., Osamura Y. & Morokuma K. 1999. Coexistence of neutral and ion-pair clusters of hydrated sulfuric acid $H_2SO_4(H_2O)_n$ (n = 1–5) — a molecular orbital study. *J. Phys. Chem. A* 103: 3535–3547.

Schwabe T. & Grimme S. 2006. Towards chemical accuracy for the thermodynamics of large molecules: new hybrid density functionals including non-local correlation effects. *Phys. Chem. Chem. Phys.* 8: 4398–4401.

Seinfeld J.H. & Pandis S.N. 1998. *Atmospheric chemistry and physics: from air pollution to climate change*. Wiley & Sons, New York, U.S.A.

Truhlar D.G. & Isaacson A.D. 1991. Simple perturbation theory estimates of equilibrium constants from force

fields. *J. Chem. Phys.* 94: 357–359.

Viisanen Y., Kulmala M. & Laaksonen A. 1997. Experiments on gas-liquid nucleation of sulfuric acid and water. *J. Chem. Phys.* 107: 920–926.

Wang N.X. & Wilson A.K. 2003. Effects of basis set choice upon the atomization energy of the second-row compounds SO_2, CCl, and ClO_2 for B3LYP and B3PW91. *J. Phys. Chem. A* 107: 6720–6724.

Weber R.J., Marti J.J., McMurry P.H., Eisele F.L., Tanner D.J. & Jefferson A. 1996. Measured atmospheric new particle formation rates: implications for nucleation mechanisms. *Chemical Engineering Communications* 151: 53–64.

Weber R.J., Marti J.J., McMurry P.H., Eisele F.L., Tanner D.J. & Jefferson A. 1997. Measurements of new particle formation and ultrafine particle growth rates at a clean continental site. *Journal of Geophysical Research D* 102: 4375–4385.

Wilson A.K., van Mourik T. & Dunning T.H.Jr. 1996. Gaussian basis sets for use in correlated molecular calculations. VI. Sextuple zeta correlation consistent basis sets for boron through neon. *J. Mol. Struct.* 388: 339–349.

Wilson A.K. & Dunning T.H.Jr. 2004. The HSO-SOH isomers revisited: the effect of tight *d* functions. *J. Phys. Chem. A* 108: 3129–3133.

Zhao Y. & Truhlar D.G. 2004. Hybrid meta density functional theory methods for thermochemistry, thermochemical kinetics, and noncovalent interactions: The MPW1B95 and MPWB1K models and comparative assessments for hydrogen bonding and van der Waals interactions. *J. Phys. Chem. A* 108: 6908–6918.

Zhao Y. & Truhlar D.G. 2005. Benchmark databases for non-bonded interactions and their use to test density functional theory. *J. Chem. Theory Comput.* 1: 415–432.

Appendix

In order to test the validity of our method, we performed a series of test calculations on the smallest cluster structures in our study: $H_2SO_4 \cdot H_2O$ and $HSO_4^- \cdot H_2O$. First, we optimized both structures at the MP2/aug-cc-pV(*D* + *d*)Z and MP2/aug-cc-pV(*T* + *d*)Z levels to test the magnitude of basis-set effects on the geometry. For the $HSO_4^- \cdot H_2O$ cluster, the minimum structures with respect to the electronic energy and the free energy at 298 K were different. Both structures (shown in Fig. A1) were analyzed here. The corresponding bond lengths, angles and binding energies are given in Table A1. The binding energies (defined as the electronic energy change for the formation reaction) at the MP2 level are given for aug-cc-pV(*D* + *d*)Z and aug-cc-pV(*T* + *d*)Z basis sets. The convergence criteria

Fig. A1. Schematic structure of the most stable one-water clusters: (**a**) $H_2SO_4 \cdot H_2O$, (**b**) $HSO_4^- \cdot H_2O$ (i) and (**c**) $HSO_4^- \cdot H_2O$ (ii).
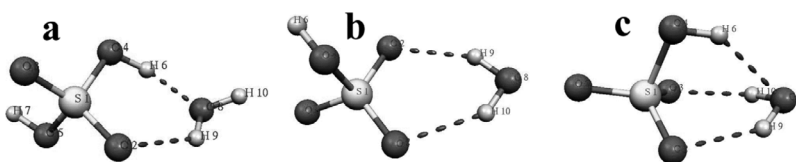
for the geometry optimizations were the Gaussian defaults: 3×10^{-4} and 4.5×10^{-4} atomic units (a.u.) with respect to the root mean square (RMS) and maximum force, respectively. The convergence with respect to the electronic energy in the self-consistent field (SCF) step was 1×10^{-6} a.u.

Next, we have calculated the MP4/aug-cc-pV(*D* + *d*)Z, MP4(SDQ)/aug-cc-pV(*D* + *d*)Z, MP4/aug-cc-pV(*T* + *d*)Z and MP4(SDQ)/aug-cc-pV(*T* + *d*)Z binding energies for both clusters at the MP2/aug-cc-pV(*D* + *d*)Z geometries (*see* Table A2 for results). The extrapolated aug-cc-pV(∞ + *d*)Z binding energies (using Eq. 2) obtained for the MP2, MP4(SDQ) and MP4 methods are given in Table A3.

It can be seen from Table A1 that the effect of going from a double-zeta to a triple-zeta basis set on the geometries is moderately small especially for the intermolecular distances, though unfortunately it is not negligible. Comparing Tables A1 and A2, it is evident that the triple-zeta corrections are important for the neutral cluster and negligibly small for the ionic clusters, while the opposite applies for the MP4 corrections. This surprising result indicates that both corrections are needed if accurate comparisons of neutral and ionic clusters are to be made. It can also be seen that the basis-set dependence of the MP2 and MP4 methods are roughly similar. Thus, our three-step extrapolation presented above can be expected to yield reasonably reliable results even though MP4/aug-cc-pV(*T* + *d*)Z binding energies are not calculated for the larger clusters. The data also shows that the MP4(SDQ) method is not a good approximation to the considerably more costly MP4 method. This is unfortunate as the computation of the triple excitations is the most time-consuming step of the MP4 energy evaluation, especially for the largest clusters.

We have also compared the basis-set limit extrapolation scheme with the other common *a posteriori* method for correcting basis-set errors, the counterpoise correction (Boys and Bernadi 1970). It is evident (Table A4) that the predicted corrections are relatively large as compared with the differences e.g. between the triple-zeta and extrapolated basis-set limit energies. Fortunately, the corrections for neutral and ionic clusters are relatively similar. Most importantly, the BSSE values calculated for the $H_2SO_4 \cdot NH_3$ and $HSO_4^- \cdot NH_3$ clusters differ by only 0.01 kcal mol⁻¹. Our conclusions on the role of ammonia in ion-induced nucleation (which depend on the difference of the ammonia addition energies) are thus not affected at all.

For correlated wavefunction-based methods, the counterpoise correction is known to often give surprisingly large BSSE values. One explanation for this is that while the counterpoise correction accurately removes the basis-set superposition error, it does not remove errors arising from basis-set incompleteness. Thus, the CP-corrected energies may actually be further from the true basis set

Table A1. Comparison of geometric parameters and binding energies obtained for the $H_2SO_4 \bullet H_2O$ and $HSO_4^- \bullet H_2O$ clusters using the MP2 method and the aug-cc-pV($D + d$)Z and aug-cc-pV($T + d$)Z basis sets. All distances (r) are in Ångströms and all angles ($\angle$) in degrees. The distances and angles corresponding to hydrogen bonds have been denoted by hb1, hb2 and hb3.

Species	$H_2SO_4 \bullet H_2O$ aug-cc-pV($D + d$)Z	$H_2SO_4 \bullet H_2O$ aug-cc-pV($T + d$)Z	$HSO_4^- \bullet H_2O$ (i) aug-cc-pV($D + d$)Z	$HSO_4^- \bullet H_2O$ (i) aug-cc-pV($T + d$)Z	$HSO_4^- \bullet H_2O$ (ii) aug-cc-pV($D + d$)Z	$HSO_4^- \bullet H_2O$ (ii) aug-cc-pV($T + d$)Z
r(S1-O2)	1.452	1.433	1.486	1.464	1.489	1.467
r(S1-O3)	1.444	1.424	1.476	1.454	1.489	1.467
r(S1-O5)	1.624	1.590	1.475	1.454	1.466	1.445
r(O5-H7)	0.974	0.969	–	–	–	–
r(S1-O4)	1.593	1.561	1.694	1.653	1.683	1.643
r(O4-H6)	1.003	1.001	0.971	0.966	0.977	0.972
r(H6···O8) (hb1)	1.683	1.654	–	–	2.250	2.227
r(H9···O2) (hb2)	2.166	2.119	2.057	2.037	2.073	2.057
r(H10···O3) (hb3)	–	–	2.115	2.108	2.073	2.057
r(O8-H10)	0.966	0.962	0.973	0.969	0.977	0.973
r(O8-H9)	0.973	0.970	0.975	0.971	0.977	0.973
$\angle$(H10-O8-H9)	105.3	105.8	97.9	97.9	98.4	98.6
$\angle$(O4-H6-O8) (hb1)	165.0	164.8	–	–	142.0	141.5
$\angle$(O8-H9-O2) (hb2)	127.8	128.1	147.5	147.3	140.8	140.4
$\angle$(O8-H10-O3) (hb3)	–	–	143.1	142.5	140.8	140.4
Binding energy	−12.73	−13.01[a] −13.02[b]	−14.77	−14.77[a] −14.75[b]	−16.16	−16.22[a] −16.17[b]

[a] Calculated at the MP2/aug-cc-pV($D + d$)Z geometry for both the cluster and the free molecules. [b] Calculated at the MP2/aug-cc-pV($T + d$)Z geometry for both the cluster and the free molecules.

Table A2. Binding energies obtained for the $H_2SO_4 \cdot H_2O$ and $HSO_4^- \cdot H_2O$ clusters using different higher-level methods, at the MP2/aug-cc-pV$(D + d)Z$ geometry. All values in kcal mol^{-1}.

Species/level	$H_2SO_4 \cdot H_2O$	$HSO_4^- \cdot H_2O$ (i)	$HSO_4^- \cdot H_2O$ (ii)
MP4(SDQ)/aug-cc-pV$(D + d)Z$	−12.11	−14.49	−15.73
MP4/aug-cc-pV$(D + d)Z$	−12.74	−15.00	−16.51
MP4(SDQ)/aug-cc-pV$(T + d)Z$	−12.36	−14.44	−15.69
MP4/aug-cc-pV$(T + d)Z$	−12.98	−14.96	−16.51

Table A3. Extrapolated basis-set limit binding energies obtained for the $H_2SO_4 \cdot H_2O$ and $HSO_4^- \cdot H_2O$ clusters using different methods. All values in kcal mol^{-1}.

Species/method	$H_2SO_4 \cdot H_2O$	$HSO_4^- \cdot H_2O$ (i)	$HSO_4^- \cdot H_2O$ (ii)
MP2	−13.13	−14.77	−16.25
MP4(SDQ)	−12.46	−14.41	−15.67
MP4	−13.08	−14.93	−16.50

limit than the uncorrected energies. To test this hypothesis, we performed a further series of test calculations with basis sets from double- to pen-tuple-zeta quality using the recently developed RI-MP2 method (Weigend and Häser 1997) with the Turbomole (ver. 5.8) program suite (Ahl-richs *et al*. 1989, Häser and Ahlrichs 1989). The RI-MP2 method employs an auxiliary basis set expansion to greatly reduce the computational effort while yielding relative (binding) energies that are essentially equal to the traditional MP2 values (*see* Weigend *et al*. (1998) for details). The auxiliary basis sets needed for the RI expansion with the aug-cc-pV$(X + d)Z$ basis sets used in this

Table A4. Basis-set superposition error corrections calculated using MP2 method and the counterpoise method for various clusters and basis sets. All geometries have been optimized at the MP2/aug-cc-pV$(D + d)Z$ level.

Cluster	Basis set	BSSE correction (kcal mol^{-1})
$H_2SO_4 \cdot H_2O$	aug-cc-pV$(D + d)Z$	+2.08
$HSO_4^- \cdot H_2O$	aug-cc-pV$(D + d)Z$	+1.69
$H_2SO_4 \cdot H_2O$	aug-cc-pV$(T + d)Z$	+1.06
$HSO_4^- \cdot H_2O$	aug-cc-pV$(T + d)Z$	+0.91
$H_2SO_4 \cdot NH_3$	aug-cc-pV$(D + d)Z$	+2.52
$HSO_4^- \cdot NH_3$	aug-cc-pV$(D + d)Z$	+2.51

study are given by Weigend *et al*. (2002). The differences between the aug-cc-pV$(D + d)Z$ and aug-cc-pV$(5 + d)Z$ binding energies (which should be quite close to the MP2 basis-set limit) are about an order of magnitude smaller than the basis-set superposition errors predicted by the counterpoise correction (Table A5). A comparison of the double- and triple-zeta values with those given in Table A1 confirms that the RI-MP2 and MP2 results are equal. For the ionic cluster, the difference between aug-cc-pV$(D + d)Z$ and aug-cc-pV$(5 + d)Z$ values is only 0.05 kcal mol^{-1}, though this is likely to be coincidental. This result is similar to that obtained by Feller (1992) who found that for a series of computations on the water dimer, application of the counterpoise correction often yielded incorrect results for correlated calculations using basis sets containing diffuse functions.

Next, we carried out a series of calculations to determine the effect of anharmonicity on the formation enthalpies and entropies. As the first approximation, the anharmonic vibrational energy levels of molecules with non-degenerate vibrations can be expressed as (Nielsen 1959, Isaacson 1998, Barone 2004):

$$E_{n_1,n_2\ldots} = X_0 + \sum_i h v_i \left(n_i + \frac{1}{2} \right) + \sum_k \sum_{i \leq k} \mathbf{X}_{i,k} \left(n_i + \frac{1}{2} \right) \left(n_k + \frac{1}{2} \right) + \ldots \tag{A1}$$

where n_i are vibrational quantum numbers, v_i is the harmonic frequency, h is the Planck constant, and $\mathbf{X}_{i,k}$ is a matrix of anharmonic constants. The constant anharmonic term X_0 effectively disappears in

the evaluation of infrared transitions. We ignore this term in the following derivations, but take it into account later as a part of ZPE. As the perturbative method for the anharmonic vibrational frequency calculations (Barone 2005) used here takes also into account Fermi resonances and correspondingly potentially divergent terms that are related to the calculation of anharmonicity constants, we adopted as ZPE not the value by Eq. A1 ($n_i = 0$) but the value proposed by Barone (2005). The corresponding correction term was also applied when Eq. A4 was used. The partition function for vibrations can be then expressed (first, for simplicity, we present the partition function for one vibration; Kvasnikov 2002):

$$Z = \sum_{n=0}^{\infty} \exp\left(-\frac{E_n}{k_b T}\right) = \sum_{n=0}^{\infty} \exp\left[-\frac{hv\left(n+\frac{1}{2}\right)+X\left(n+\frac{1}{2}\right)^2}{k_b T}\right] = \sum_{n=0}^{\infty}\left\{\exp\left[-\zeta\left(n+\frac{1}{2}\right)\right]\left[1-\chi\left(n+\frac{1}{2}\right)^2\right]\right\} \quad (A2)$$

$$= Z_0 - \chi\frac{d^2}{d\zeta^2}Z_0$$

where Z_0 denotes the partition function of harmonic vibration, $\zeta = hv/k_b T$ and $\chi = X/k_b T$. For a collection of vibrations this expression can be generalized:

$$Z = Z_0 - \sum_k \sum_{i \leq k} \chi_{i,k} \frac{d}{d\zeta_i}\frac{d}{d\zeta_k}Z_0 \quad (A3)$$

From which it follows that the anharmonicity-corrected internal energy E_{vib} and entropy S_{vib} (per molecule) is:

$$E_{vib} = \sum_k hv_k f\left(\zeta_k\right) + \sum_k X_{k,k}\left\{\tfrac{1}{4} + 2\left[f\left(\zeta_k\right)^2 - \frac{1}{4}\right]\left[1-2\zeta_k f\left(\zeta_k\right)\right]\right\}$$

$$+ \sum_k \sum_{i<k}\left\{X_{i,k} f\left(\zeta_i\right)f\left(\zeta_k\right)\left[1+\frac{2\zeta_i}{e^{-\zeta_i}-e^{\zeta_i}}+\frac{2\zeta_k}{e^{-\zeta_k}-e^{\zeta_k}}\right]\right\}, \quad (A4)$$

where $f(\zeta) = 1/2 + (e^\zeta - 1)^{-1}$, and

$$\frac{S_{vib}}{k_b} = \sum_i\left[\frac{\zeta_i}{e^{\zeta_i}-1} - \ln\left(1-e^{-\zeta_i}\right)\right] - 2\sum_i\left[\zeta_i\chi_{i,i}\frac{e^{\zeta_i}\left(e^{\zeta_i}+1\right)}{\left(e^{\zeta_i}-1\right)^3}\right]$$

$$+ \sum_k \sum_{i<k}\chi_{i,k}\left[f\left(\zeta_i\right)f\left(\zeta_k\right)\left(\frac{2\zeta_i}{e^{-\zeta_i}-e^{\zeta_i}}+\frac{2\zeta_k}{e^{-\zeta_k}-e^{\zeta_k}}\right)\right] \quad (A5)$$

The first terms in these expressions represent internal energy and entropy in the harmonic approximation.

It is a common practice to calculate thermal contributions to the enthalpy and entropy that approximately take into account anharmonicity by using anharmonic fundamental frequencies in expressions

Table A5. Reaction energies for the addition of a water molecule to sulfuric acid and the hydrogensulfate ion, computed using the RI-MP2 method and three different basis sets. All geometries have been optimized at the MP2/aug-cc-pV($D + d$)Z level.

Basis set	ΔE_0 (kcal mol^{-1}) for the reaction $H_2SO_4 + H_2O \Rightarrow H_2SO_4 \bullet H_2O$	ΔE_0 (kcal mol^{-1}) for the reaction $HSO_4^- + H_2O \Rightarrow HSO_4^- \bullet H_2O$
aug-cc-pV($D + d$)Z	−12.73	−14.77
aug-cc-pV($T + d$)Z	−13.02	−14.78
aug-cc-pV(Q + d)Z	−12.91	−14.65
aug-cc-pV(5 + d)Z	−12.78	−14.51

that are derived for harmonic frequencies (*see* for example McQuarrie 1976, Truhlar and Isaacson 1991, Barone 2004). The Gaussian 03 program package (Frisch *et al.* 2004) calculates anharmonic constants X_{ij} using a perturbative approach (Barone 2005), but the computational costs increase rapidly for larger molecules. It should be noted that the anharmonic thermochemical contributions given by the Gaussian program are calculated simply by using anharmonic vibrational frequencies in the harmonic expressions.

To account for anharmonicity in larger molecules, it is rather common to introduce scaling factors for harmonic frequencies to estimate fundamental frequencies and anharmonic corrections to thermochemical parameters. The values of these factors are usually determined by comparison with credible experimental data (Scott and Radom 1996). We calculated the anharmonic constants for the H_2O and H_2SO_4 molecules and the $H_2SO_4 \bullet H_2O$ and $H_2SO_4 \bullet (H_2O)_2$ clusters at the MP2/aug-cc-pV($D + d$)Z level using the perturbative method implemented in the Gaussian 03 program. Anharmonic contributions to thermochemical parameters were computed both by using the fundamental (anharmonic) frequencies in the harmonic expressions, and with Eqs. A4 and A5 (the second and third terms) (*see* Table A6).

We also attempted to calculate anharmonic vibrational frequencies for the HSO_4^- ion and the $HSO_4^- \bullet H_2O$ (i), $HSO_4^- \bullet H_2O$ (ii) and $HSO_4^- \bullet (H_2O)_2$ (i) and $HSO_4^- \bullet (H_2O)_2$ (ii) clusters. However, upon inspection of the results we discovered that one of the anharmonic vibrational frequencies for the HSO_4^- ion was negative. The reported anharmonic wavenumber was -12.286 cm^{-1}, while the corresponding har-

Table A6. Zero-point energies (ZPE) and thermal contributions to the enthalpies H_{therm} (defined as $H(T) - E_0$), entropies S, and Gibbs free energies G_{therm} (defined as $G(T) - E_0$) calculated at the MP2/aug-cc-pV($D + d$)Z level, at a temperature of 298 K and a reference pressure of 1 atm, using various treatments for the vibrational modes. The first column ("harmonic") corresponds to the harmonic vibrational approximation. The values in the second column (Anharmonic value, fundamentals) have been calculated using the anharmonic fundamental vibrational frequencies in the harmonic expressions, and the values in the third column (Anharmonic value, Eqs. A4 and A5) have been calculated using the computed anharmonicity constants in Eqs. A4 and A5, given above. Also reported is the average ratio of the anharmonic and harmonic fundamental frequencies, $\Sigma v_{fund}/\Sigma v_{harm}$.

Parameters	Harmonic value	Anharmonic value, fundamentals	Anharmonic value, Eqs. A4 and A5
H_2O			
ZPE (kcal mol^{-1})	13.39	13.17	13.17
$\Sigma v_{fund}/\Sigma v_{harm}$		0.95454	
H_{therm} (kcal mol^{-1})	15.76	15.54	15.54
S (cal Kmol^{-1})	45.12	45.12	45.12
G_{therm} (kcal mol^{-1})	2.30	2.09	2.09
H_2SO_4			
ZPE (kcal mol^{-1})	24.27	23.93	23.93
$\Sigma v_{fund}/\Sigma v_{harm}$		0.96194	
H_{therm} (kcal mol^{-1})	28.12	27.88	27.93
S (cal Kmol^{-1})	71.16	71.78	71.97
G_{therm} (kcal mol^{-1})	6.91	6.48	6.47
$H_2SO_4 \bullet H_2O$			
ZPE (kcal mol^{-1})	39.91	39.20	39.20
$\Sigma v_{fund}/\Sigma v_{harm}$		0.95006	
H_{therm} (kcal mol^{-1})	45.51	45.06	45.48
S (cal Kmol^{-1})	87.13	89.42	91.33
G_{therm} (kcal mol^{-1})	19.54	18.40	18.25
$H_2SO_4 \bullet (H_2O)_2$			
ZPE (kcal mol^{-1})	55.74	54.65	54.65
$\Sigma v_{fund}/\Sigma v_{harm}$		0.94403	
H_{therm} (kcal mol^{-1})	63.02	62.34	62.94
S (cal Kmol^{-1})	101.35	105.21	107.55
G_{therm} (kcal mol^{-1})	32.81	30.98	30.88

continuned

Table A6. Continued.

Parameters	Harmonic value	Anharmonic value, fundamentals	Anharmonic value, Eqs. A4 and A5
HSO$_4^-$			
ZPE (kcal mol^{-1})	16.48[a]	16.23	16.23
$\Sigma\nu_{fund}/\Sigma\nu_{harm}$		0.95961	
H_{therm} (kcal mol^{-1})	20.23[a]	19.86	19.85
S (cal Kmol^{-1})	72.77[a]	71.98	71.94
G_{therm} (kcal mol^{-1})	−1.47[a]	−1.60	−1.60
HSO$_4^-$·H$_2$O (i)			
ZPE (kcal mol^{-1})	31.94[a]	31.41	31.41
$\Sigma\nu_{fund}/\Sigma\nu_{harm}$		0.94984	
H_{therm} (kcal mol^{-1})	37.64[a]	36.93	37.44
S (cal Kmol^{-1})	89.88[a]	92.78	94.43
G_{therm} (kcal mol^{-1})	10.84[a]	9.27	9.30
HSO$_4^-$·H$_2$O (ii)			
ZPE (kcal mol^{-1})	32.74	32.15	32.15
$\Sigma\nu_{fund}/\Sigma\nu_{harm}$		0.93205	
H_{therm} (kcal mol^{-1})	37.94	37.60	37.93
S (cal Kmol^{-1})	84.47	86.58	88.17
G_{therm} (kcal mol^{-1})	12.76	11.79	11.64
HSO$_4^-$·(H$_2$O)$_2$ (i)			
ZPE (kcal mol^{-1})	48.10	47.21	47.21
$\Sigma\nu_{fund}/\Sigma\nu_{harm}$		0.94297	
H_{therm} (kcal mol^{-1})	55.34	54.79	55.03
S (cal Kmol^{-1})	102.38	105.46	106.20
G_{therm} (kcal mol^{-1})	24.81	23.34	23.36
HSO$_4^-$·(H$_2$O)$_2$ (ii)			
ZPE (kcal mol^{-1})	48.90	47.91	47.91
$\Sigma\nu_{fund}/\Sigma\nu_{harm}$		0.93743	
H_{therm} (kcal mol^{-1})	55.57	54.97	56.01
S (cal Kmol^{-1})	96.82	100.83	106.03
G_{therm} (kcal mol^{-1})	26.70	24.91	24.39

[a] Calculated using the harmonic approximation, ignoring internal rotations.

monic wavenumber was 104.373 cm^{-1}. Visual inspection of the normal mode in question showed that it resembles a hindered internal rotation of the hydrogen atom around the S–OH bond. We then attempted to use the hindered rotor analysis package of the Gaussian 03 program (Ayala and Schlegel 1998). The program identified the internal rotation, but unfortunately failed before completing the analysis. We are as yet unable to determine precisely the cause of the failure. We computed anharmonic contributions to the entropy and enthalpy of the HSO$_4^-$ ion by using the approximation of a simple hindered rotor with a periodic potential for the lowest normal mode and with Eqs. A4 and A5 with the anharmonicity constants for all the other modes. Applying the method by Pitzer (1946) we calculated the reduced moment of inertia around bond HO–SO$_3$ to be $I_r = 0.943$ amu Å^2 (actually, the axis through mass centers of OH and SO$_3$ was used). The periodicity of the internal rotation potential and symmetry number of rotator was assumed to be 3. The barrier height was derived from the harmonic wavenumber and symmetry number (eq. 13 in Ayala and Schlegel 1998). We calculated the entropy and enthalpy of hindered rotation using the tables of Pitzer and Gwinn (1942) (*see* Table A6).

    One of the anharmonic overtone frequencies of the HSO$_4^-$•H$_2$O (i) cluster was also negative, though all the fundamental frequencies were positive. The structure of the cluster (*see* Fig. A1) indicates that this may also be related to an internal rotation around the S–OH bond, though a clearly corresponding normal mode was not found in the frequency visualization. We applied the above-described procedure also for HSO$_4^-$•H$_2$O (i). The periodicity of the internal rotation potential was

assumed to be 3, but due to the presence of the water molecule, the symmetry number was assumed to be 1. The obtained reduced moment of inertia I_r = 0.938 amu Å² for the HSO_4^-•H_2O (i) cluster is similarly to HSO_4^-. As a first approximation, we have computed the thermochemical parameters for HSO_4^-•H_2O (i) similarly to HSO_4^-. The HSO_4^-•H_2O (ii) cluster did not possess any internal rotations, and the data computed for this cluster should thus be considered more reliable.

As can be seen from Table 2, accounting for the presence of internal rotations for HSO_4^- and HSO_4^-•H_2O (i) improved the match between experimental and computed results.

The computed anharmonic thermal contributions to the enthalpy, entropy and zero-point energies were used to determine two sets of scaling factors: sf1 and sf2 (*see* Table A7). The sf1 set is fitted to the column "Anharmonic value, fundamentals" (Table A6), while the sf2 set is fitted to the column "Anharmonic value, Eqs. A4 and A5". It can be seen (Tables A6 and A7) that both anharmonicity treatments give practically identical corrections for the small water molecule, while the corrections are rather different for the enthalpy and entropy of sulfuric acid mono- and dihydrate. However, the corrections for the free energy differ less, the application of Eqs. A4 and A5 yielding e.g. a 0.15 kcal mol⁻¹ more negative value for the monohydrate. We see also that the scaling factors corresponding to the more accurate anharmonicity treatment are considerably lower than those corresponding to the approximate "fundamental frequencies" treatment. It is also evident (Tables A6 and A7) that the effect of anharmonicity at the MP2/aug-cc-pV(D + d)Z level is rather large and should be taken into account in hydrate distribution calculations. The anharmonicity also increases with the size of the system. This is logical, as the loose intermolecular vibrational modes of the cluster structures are likely to be more anharmonic (at least with respect to their entropy and enthalpy contributions). The dihydrate clusters seem to be slightly more anharmonic than the monohydrates, implying that the larger clusters might be more anharmonic still. However, the differences between two ionic dihydrates are about as large as the average difference between the ionic dihydrates and the ionic monohydrate. This is probably an indication of the limitations of the scaling factor approach.

We have not calculated the scaling factors sf1 and sf2 for the ions HSO_4^- and HSO_4^-•H_2O (i) as they contain internal rotations. In all calculations on larger clusters, the scaling factors for the most stable dihydrates were used: H_2SO_4•$(H_2O)_2$ for the neutral clusters and HSO_4^-•$(H_2O)_2$ (i) for the ionic clusters. Use of the scaling factors derived for the considerably more anharmonic HSO_4^-•$(H_2O)_2$ (ii) isomer for the larger ionic clusters would change the entropies by up to 11.5% and the enthalpies and Gibbs free energies by up to 1.5%, as discussed below. This treatment is highly approximate, but due to the enormous computational effort required to compute anharmonic corrections for large cluster systems it is the only affordable possibility.

The *ab initio* calculations have shown that hydrates with the same stoichiometry can have many stable structures (defined as minima on the

Table A7. Scaling factor sets sf1 and sf2 determined for each molecule and thermochemical parameter. *See* text for details.

Species	sf1	sf2
H₂O		
ZPE$_{tot}$/ZPE$_{harm}$	0.98378	0.98378
H_{therm}	0.96947	0.97221
S	0.96947	0.97226
H₂SO₄		
ZPE$_{tot}$/ZPE$_{harm}$	0.98603	0.98603
H_{therm}	0.95531	0.93520
S	0.95049	0.93693
H₂SO₄•H₂O		
ZPE$_{tot}$/ZPE$_{harm}$	0.98203	0.98203
H_{therm}	0.91832	0.80712
S	0.90108	0.83024
H₂SO₄•(H₂O)₂		
ZPE$_{tot}$/ZPE$_{harm}$	0.98056	0.98056
H_{therm}	0.90648	0.78790
S	0.88369	0.82308
HSO₄⁻•H₂O (ii)		
ZPE$_{tot}$/ZPE$_{harm}$	0.98216	0.98216
H_{therm}	0.92030	0.82411
S	0.89873	0.83342
H₂SO₄⁻•(H₂O)₂ (i)		
ZPE$_{tot}$/ZPE$_{harm}$	0.98135	0.98135
H_{therm}	0.91454	0.86086
S	0.90229	0.88126
H₂SO₄⁻•(H₂O)₂ (ii)		
ZPE$_{tot}$/ZPE$_{harm}$	0.97986	0.97986
H_{therm}	0.90531	0.70412
S	0.86852	0.73542

potential energy surface of the nuclei). As the number and type of stable structures found for some stoichiometry is almost always somewhat arbitrary (unless a full conformational sampling is carried out e.g. by monte carlo methods, which is computationally impossible for the quantum chemical methods used in this study), thermochemical parameters are usually computed using only the "best" minimum structures (i.e. those with the lowest electronic or free energy). We investigated the effect of the presence of multiple conformers on the computed enthalpies (H_i) and entropies (S_i) of the ionic hydrates. The ionic hydrates were selected as there is experimental data available for all four hydration reactions, not just the first two. We considered the transfer between conformers A and B as a chemical reaction A ↔ B. The rate of this reaction depends on the heights of the energy barriers of the isomerization pathways between these conformers, and may thus be very slow. In other words, the time needed to reach the equilibrium state between conformers may be very long. Here, we nevertheless assume that the different conformers are in the equilibrium. The equilibrium constant of isomerization reaction can be expressed as:

$$K_{A \leftrightarrow B} = \frac{\rho_B}{\rho_A} \tag{A6}$$

and

$$\ln\left(K_{A \leftrightarrow B}\right) = -\frac{G_B - G_A}{RT} = -\frac{\left(H_B - TS_B\right) - \left(H_A - TS_A\right)}{RT}, \tag{A7}$$

where ρ_A and ρ_B are the number concentrations of conformers A and B, respectively; G_A and G_B are the corresponding standard Gibbs' free energies. The fraction x_k of the kth conformer is given by

$$x_k = \frac{\rho_k}{\sum_l \rho_l} = \frac{1}{1 + \sum_{l \neq k} K_{k \leftrightarrow l}}. \tag{A8}$$

The enthalpy and entropy of the mixture of conformers can be now calculated as

$$H = \sum_k x_k H_k \tag{A9}$$

and

$$S = \sum_k x_k S_k \tag{A10}$$

respectively. Comparing Tables 2 and A8 it can be seen that while ensemble averaging (or using a different set of scaling factors) may decrease the difference between computed and experimental values for some reactions, none of the datasets matches all of the experimental values. Specifically, no combination of ensemble-averaging and scaling is able to predict correctly the entropy and enthalpy changes for the $HSO_4^- \bullet (H_2O)_3 + H_2O => HSO_4^- \bullet (H_2O)_4$ (though the errors in the entropies and enthalpies act in opposite directions, so that the errors in the free energy change are mostly cancelled out). This might be related to the presence of unidentified internal rotations in the $HSO_4^- \bullet (H_2O)_4$ clusters.

References for the Appendix

Ahlrichs R., Bär M., Häser M., Horn H. & Kölmel C. 1989. Electronic structure calculations on workstation computers: The program system Turbomole. *Chem. Phys. Lett.* 162: 165–169.

Ayala P.Y. & Schlegel H.B. 1998. Identification and treatment of internal rotation in normal mode vibrational analysis. *J. Chem. Phys.* 108: 2314–2325.

Häser M. & Ahlrichs R. 1989. Improvements on the direct SCF method, *J. Comput. Chem.* 10: 104–111.

Isaacson A.D. 1998. Removing resonance effects from quantum mechanical vibrational partition functions obtained from perturbation theory. *J. Chem. Phys.* 108: 9978–9986.

Kvasnikov I.A. [Квасников, И. А.] 2002. *Thermodynamics and statistical physics, vol. 2: Theory of equilibrium systems: Sta-*

Table A8. Reaction thermodynamics computed for water addition reactions to ionic clusters at 298 K and a reference pressure of 1 atm, using ensemble-averaged values for the thermochemical parameters.

Reaction	ΔS, 298K (cal Kmol^{-1})	ΔH, 298K (kcal mol^{-1})	ΔG, 298K (kcal mol^{-1})
$HSO_4^- + H_2O \Rightarrow HSO_4^- \bullet H_2O$	−30.03[a]	−13.78[a]	−4.83[a]
	−25.45[b]	−13.61[b]	−6.03[b]
	−24.05[c]	−13.78[c]	−6.61[c]
	−23.0[d]	−12.9[d]	
$HSO_4^- \bullet H_2O + H_2O \Rightarrow HSO_4^- \bullet (H_2O)_2$	−33.68[a]	−13.71[a]	−3.67[a]
	−34.12[b]	−13.71[b]	−3.52[b]
	−32.46[c]	−13.00[c]	−3.32[c]
	−22.0[d]	−11.2[d]	
$HSO_4^- \bullet (H_2O)_2 + H_2O \Rightarrow HSO_4^- \bullet (H_2O)_3$	−36.47[a]	−13.67[a]	−2.79[a]
	−34.45[b,e]	−13.14[b,e]	−3.32[b,e]
	−35.99[b,f]	−13.09[b,f]	−2.86[b,f]
	−31.09[c,e]	−12.94[c,e]	−3.67[c,e]
	−38.10[c,f]	−13.82[c,f]	−2.46[c,f]
	−30.7[d]	−12.4[d]	
$HSO_4^- \bullet (H_2O)_3 + H_2O \Rightarrow HSO_4^- \bullet (H_2O)_4$	−26.87[a]	−9.70[a]	−1.69[a]
	−25.34[b,e]	−9.68[b,e]	−2.13[b,e]
	−25.76[b,f]	−9.67[b,f]	−1.99[b,f]
	−23.40[c,e]	−9.43[c,e]	−2.45[c,e]
	−25.49[c,f]	−9.61[c,f]	−2.01[c,f]
	−36.3[d]	−13.2[d]	

[a] Harmonic values, internal rotations are ignored. [b] Anharmonic values using the sf1 scaling factor, assuming an internal rotation for HSO_4^- and $HSO_4^- \bullet H_2O$ (i). [c] Anharmonic values using the sf2 scaling factor set, assuming an internal rotation for HSO_4^- and $HSO_4^- \bullet H_2O$ (i). [d] Experimental values, Froyd and Lovejoy (2003). [e] Scaling factors taken from the $HSO_4^- \bullet (H_2O)_2$ (ii) isomer. [f] Scaling factors taken from the $HSO_4^- \bullet (H_2O)_2$ (i) isomer.

tistical physics. Editorial URSS, Moscow. [In Russian].

McQuarrie D.A. 1976. *Statistical mechanics*. Harper & Row, New York, USA.

Nielsen H.H. 1959. The vibration-rotation energies of molecules and their spectra in the infra-red. *Encyclopedia of Physics*. 37: 173–311, Springer-Verlag, Berlin, Germany.

Pitzer K.S. 1946. Energy levels and thermodynamic functions for molecules with internal rotation II. Unsymmetrical tops attached to a rigid frame. *J. Chem. Phys.* 14: 239–243.

Pitzer K.S. & Gwinn W.D. 1942. Energy levels and thermodynamic functions for molecules with internal rotation I. Rigid frame with attached tops. *J. Chem. Phys.* 10: 428–440.

Scott A.P. & Radom L. 1996. Harmonic vibrational frequencies: an evaluation of hartree-fock, møller-plesset, quadratic configuration interaction, density functional theory, and semiempirical scale factors. *J. Phys. Chem.* 100: 16502–16513.

Truhlar D. G. & Isaacson A.D. 1991. Simple perturbation theory estimates of equilibrium constants from force fields. *J. Chem. Phys.* 94: 357–359.

Weigend F. & Häser M. 1997. RI-MP2: first derivatives and global consistency. *Theor. Chem. Acc.* 97: 331–340.

Weigend F., Häser M., Patzelt H. & Ahlrichs R. 1998. RI-MP2: Optimized auxiliary basis sets and demonstration of efficiency. *Chem. Phys. Lett.* 294: 143–152.

Weigend F., Köhn A. & Hättig C. 2002. Efficient use of the correlation consistent basis sets in resolution of the identity MP2 calculations. *J. Chem. Phys.* 116: 3175–3183.